ACS OMEGA

Open Access

http://pubs.acs.org/journal/acsodf

Article

Photothermal Hydrogel Composites Featuring G4-Carbon Nanomaterial Networks for *Staphylococcus aureus* Inhibition

Monica-Cornelia Sardaru, Irina Rosca, Cristian Ursu, Ioan-Andrei Dascalu, Elena-Laura Ursu, Simona Morariu, and Alexandru Rotaru*

Cite This: *ACS Omega* 2024, 9, 15833−15844

Read Online

ACCESS | Metrics & More | Article Recommendations | Supporting Information

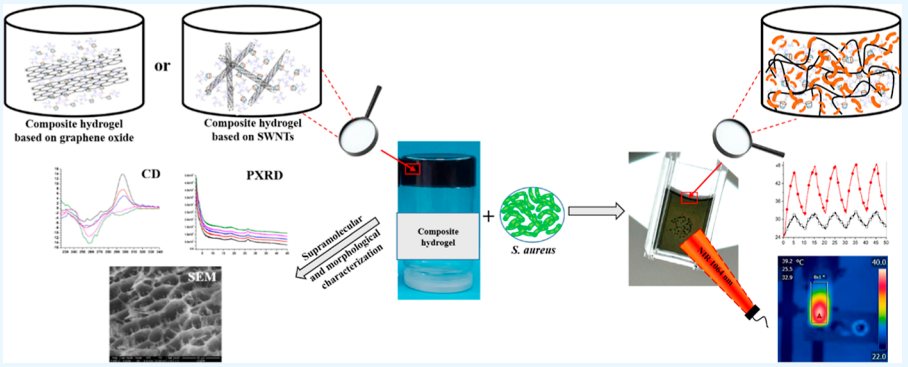

ABSTRACT: Microbial infections represent a significant health risk, often leading to severe complications and, in some cases, even fatalities. As a result, there is an urgent need to explore innovative drug delivery systems and alternative therapeutic techniques. The photothermal therapy has emerged as a promising antibacterial approach and is the focus of this study. Herein, we report the successful synthesis of two distinct supramolecular composite hydrogels by incorporating graphene oxide (GO) and single-walled carbon nanotubes (SWNTs) into guanosine quadruplex (G4) based hydrogels containing covalently bound β-cyclodextrin (β-CD). The G4 matrix was synthesized through a two-step process, establishing a robust network between G4 and β-CDs, followed by the encapsulation of either GO or SWNTs. Comprehensive characterization of these composite hydrogels were conducted using analytical techniques, including circular dichroism, Raman spectroscopy, rheological investigations, X-ray diffraction, and scanning electron microscopy. A notable discovery from the conducted research is the differential photothermal responses exhibited by the hydrogels when exposed to near-infrared laser irradiation. Specifically, SWNT-based hydrogels demonstrated superior photothermal performance, achieving a remarkable temperature increase of up to 52 °C, in contrast to GO-based hydrogels, which reached a maximum of 34 °C. These composite hydrogels showed good cytotoxicity evaluation results and displayed synergistic antibacterial activity against *Staphylococcus aureus*, positioning them as promising candidates for antibacterial photothermic platforms, particularly in the context of wound treatment. This study offers a valuable contribution to the development of advanced and combined therapeutic strategies for combating microbial infections and highlights the potential of carbon nanomaterial-enhanced supramolecular hydrogels in photothermal therapy applications.

1. INTRODUCTION

Bacterial infections pose a significant threat to human health, presenting a substantial global challenge that endangers public well-being and places a substantial economic burden on society.[1−3] During the twentieth century and the early years of the twenty-first century, antibiotics were the primary choice for treating infectious diseases, serving as the foundation of modern medicine's approach to combatting bacterial infections.[4,5] However, the irresponsible utilization and administration of antibiotics have caused the antibiotic tolerance and resistance[6,7] and highlighted the importance of researching alternative therapeutic techniques. Such efforts are focused not only on combating more efficiently bacterial infections but also on reducing the chance of developing antimicrobial resistance.[8] Among the available alternatives, the rapid evolution of nanotechnology has presented novel opportunities for the utilization of physical antimicrobial techniques, offering a wider range of prospects for their implementation.[8,9] A specific focus within available novel approaches incorporating nanomaterials

Received: October 5, 2023
Revised: March 6, 2024
Accepted: March 20, 2024
Published: March 29, 2024

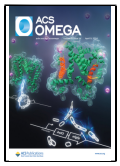

Scheme 1. Schematic Representation of Composite Hydrogels Based on Graphene-Oxide (G4-GO_1-5) and SWNTs (G4-CNT_1-5)

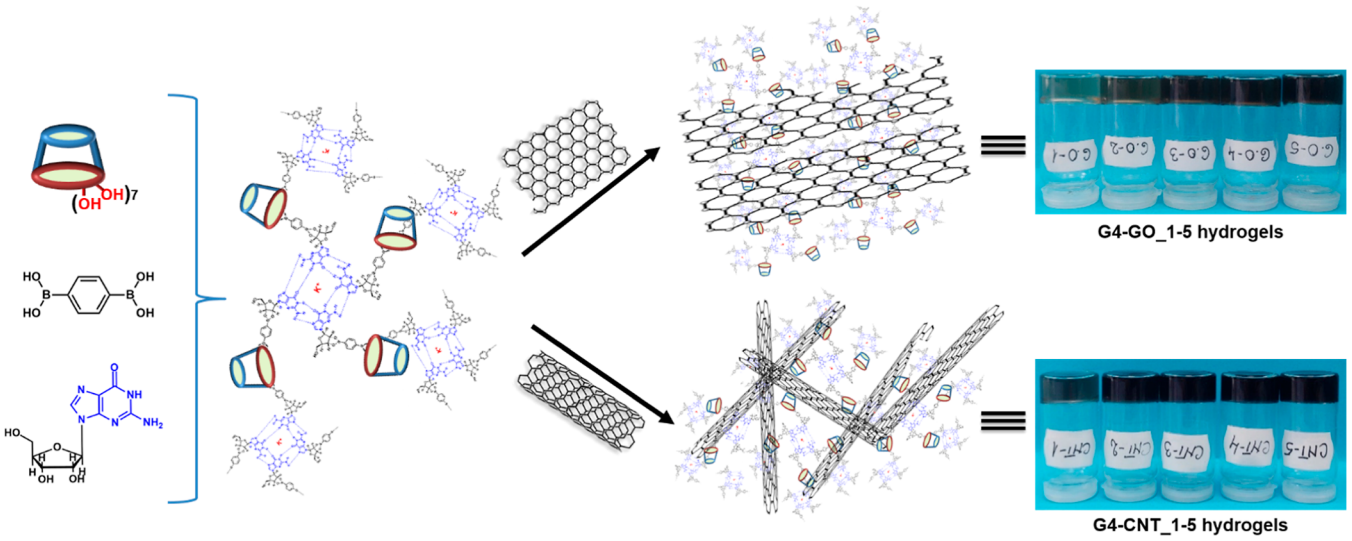

is represented by photothermal properties, where a hyperthermic response is induced through irradiation with light of a specific wavelength.[10] The developed technique named photothermal therapy is considered an optimal antibacterial therapy due to its capacity to minimize tissue damage, accelerate treatment duration, enhance permeability, and reduce the occurrence of side effects.[11−13] Upon exposure to light, specifically designed nanomaterial-based systems produce localized heat in their immediate surroundings, causing damage to both the bacteria and the formed biofilms through perturbation of bacteria's cell membranes, protein denaturation, and degradation of nucleic acids.[10,14−18]

Graphene oxide (GO) and carbon nanotubes, commercially available nanomaterials, have found extensive applications due to their distinctive physicochemical characteristics.[16,19−23] GO is a two-dimensional carbon-based nanomaterial that exhibits remarkable photothermal characteristics due to its extensive surface area and excellent light absorption. The hydrophilic nature of GO allows it to demonstrate significant dispersion in aqueous solutions, as well as possess minimal cytotoxicity and good biocompatibility.[24−28] The antibacterial impact of GO is manifested by its aggregation onto the bacterial surface, inducing detrimental effects on bacterial membranes, primarily attributed to the sharp edges present on the GO nanosheets.[29−31] Single-walled carbon nanotubes (SWNTs) on the other hand are cylindrical nanostructures composed of carbon atoms. Their distinct physical and chemical properties have garnered considerable interest in diverse domains, particularly in medicine and biotechnology.[32,33] Research on the antibacterial properties of SWNTs revealed their potential to impede the proliferation of specific bacterial strains due to their acute edges which improves their capacity to penetrate bacterial cell barriers and cause extensive damage.[34]

One common strategy to enhance the efficacy of GO and SWNTs and to broaden their applications in, for example, wound dressing, is their encapsulation into hydrogels.[28,35,36] Hydrogels represent the optimal choice for wound healing dressings due to their similitude to the extracellular matrix, remarkable recoverability, and exceptional biocompatibility.[37,38] In particular, the supramolecular hydrogels, the three-dimensional structures that contain a considerable amount of water or biological fluids, and are typically constructed involving relatively weak cross-linking forces, such as hydrogen bonding, metal coordination, host−guest interaction, $\pi-\pi$ interactions, etc.[37,39−41] These dynamic systems can be ideal for biomedical applications due to their high biocompatibility, porous structure, and tunable elastic property.[42,43] Supramolecular hydrogels used as agents in wound healing therapy present a series of benefits such as creating a moist environment, accelerating wound closure, reducing pain, minimizing scarring, and promoting tissue regeneration.[44] The combination of supramolecular hydrogels and carbon nanomaterials not only provides a means to finely tune the mechanical properties of the hydrogel but also introduces a stimuli responsiveness to the final material. Light irradiation, employed as a stimulus for temperature increase, has the potential to impact the dynamic nature of the hydrogel and holds the possibility of enhancing the rate of drug release or producing a controlled and on-demand therapeutic effect.

Recently, we reported the successful preparation of an injectable supramolecular hydrogel based on β-cyclodextrin (β-CD), cross-linked by guanosine quartets (G4), with selective antimicrobial properties.[45] The proposed synthetic pathway enables precise and controllable covalent integration of β-CD entities within the supramolecular matrix, affording the ability to fine-tune its physical characteristics. The antimicrobial properties of the reported hydrogels against *Staphylococcus aureus* (*S. aureus*) owed to the specific action of substituted β-CD over the integrity of Gram-positive bacteria membranes.[46,47] Furthermore, we have previously highlighted the promising potential of G4-based hydrogels in effectively dispersing and stabilizing variable quantities of SWNTs, resulting in a significant enhancement of the hydrogels' mechanical properties.[48]

Herein, we report on successful incorporation of controlled amounts of GO and SWNTs into the G4 hydrogels containing β-CD, resulting in two distinct sets of composite hydrogels with a variable content of nanomaterials. The hydrogel matrix was prepared in a two-step procedure by reacting 1 equiv of benzene-1,4-diboronic acid and β-CD in the presence of KOH, followed by the reaction with the equivalent amount of guanosine. The presence of potassium ions in the reaction

https://doi.org/10.1021/acsomega.3c07724
ACS Omega 2024, 9, 15833−15844

medium led to guanosine self-assembly into G4, creating an extended network between G4 and β-CDs with the formation of the hydrogel (Scheme 1). Various quantities of GO were directly incorporated into the hydrogel, whereas SWNTs, prior to their integration into the hydrogel, were initially dispersed within a nongelled hydrogel matrix prepared with LiOH. The prepared GO and SWNT composite hydrogels have been characterized using circular dichroism (CD), Raman spectroscopy, rheological measurements, X-ray diffraction, and scanning electron microscopy (SEM), including the assessment of their photothermal and antibacterial properties.

These composite hydrogels demonstrated synergistic antibacterial activity against *S. aureus* upon laser irradiation at 1064 nm and hold promise as a novel antibacterial photothermic platform for treating bacterial infections in wounds. Moreover, the presence of noncomplexed β-CD supramolecular networks not only facilitated the integration of carbon nanomaterials into the hydrogel matrix but also holds the potential to act as a carrier for water-insoluble drugs and serve as an inspiration for designing future more intricate antimicrobial systems.

2. RESULTS AND DISCUSSION

2.1. Preparation and Characterization of Hydrogels.

Two distinct series of novel composite supramolecular hydrogels have been successfully synthesized (Scheme 1). The proposed systems were based on a rational design closely related to the structural particularities of the components and especially the general structure of the hydrogel. In the initial phase, a β-CD supramolecular hydrogel was prepared and utilized for the insertion of carbon nanomaterials. This hydrogel was prepared following recently reported protocol[45] involving reactions between 1,4-benzene diboronic acid, β-CD, and guanosine in appropriate stoichiometric ratios. Subsequently, the necessary amount of a stock solution containing SWNTs or GO was added to yield a final series of composite materials. The presence in solution of the K^+ ions ensures the formation of the extensive network of G4 thus "reticulating" the whole system into strong hydrogels.[40,49−51]

A set of five hydrogels (G4-CNT_1−5) with varying concentrations of SWNTs (0.1 0.3, 0.5, 0.7, and 1 mg) were prepared by combining different volumes of SWNT stock solution of LiOH-based nongelled hydrogel matrix. Correspondingly, five hydrogels (G4-GO_1−5) containing distinct amounts of GO (0.1 0.3, 0.5, 0.7, and 1 mg) were prepared by adding GO water stock solution. Both sets of hydrogels displayed uniformly dispersed carbon nanomaterials stable over a long period of time (Scheme 1).

For formulations that utilize GO, the underlying mechanism for the successful inclusion of the nanomaterial into the hydrogel matrix relies on its structural particularities. GO, characterized as an amphiphilic layer, exhibits a monolayer configuration with a sp^2 carbon atom arrangement, enriched with numerous oxygen-bearing functional groups. The hydrogen-bonding dynamics between the carboxyl entities on GO's surface and the hydroxyl units on β-CD facilitate the creation of strong hydrogels that possess distinct characteristics.[52,53]

When considering SWNTs, which represent a rolled up graphite sheet into a tubular structure, β-CD molecules absorb themselves alongside the nanotubes[54] by the van der Waals force as was previously demonstrated in the case of β-CD and γ-CD.[55,56] This interaction, together with the hydrophobic nature of the G4 network, leads to both the stabilization and dispersion of SWNTs in the hydrogel, eliminating the disadvantage of SWNTs aggregating in an aqueous medium.[48]

To gain a deeper insight into the dispersion process within the hydrogel matrix, Raman spectroscopy analyses were conducted for all of the synthesized samples (Figures 1 and S1).

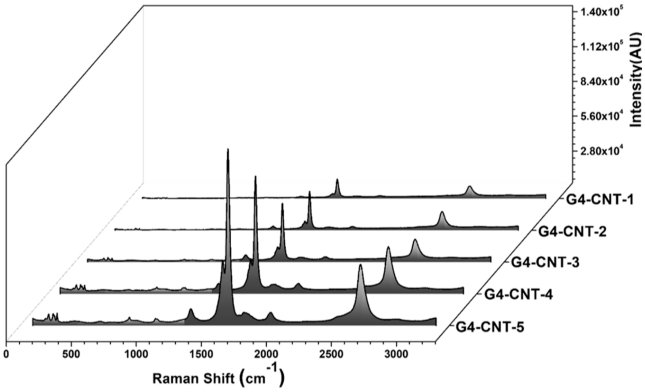

Figure 1. Raman spectra of the G4-CNT_1−5 hydrogels.

In the Raman spectra of the G4-GO_1−5 hydrogels (Figure S1), two distinct spectral peaks were detected at wavenumbers 1358 and 1598 cm^{-1}, corresponding to the D and G bands. The emergence of the D band is attributed to the presence of structural defects within the functional groups, resulting in vibrational activity among the sp^3 carbon atoms. Conversely, the G band signifies the first-order scattering of E_{2g} phonons in sp^2 carbon atoms, indicative of the presence of graphitic domains.[57,58] Likewise, in the Raman spectra of hydrogels based on SWNTs (G4-CNT_1−5, Figure 1), G (1317 cm^{-1}), D (1600 cm^{-1}), and D′ (2620 cm^{-1}) bands were evidenced.[48,59] Moreover, the bands corresponding to the SWNT radial breathing mode (220−285 and 150−210 cm^{-1}) were observed in the Raman spectra for concentrations higher than 0.5 mg. Upon analyzing the spectra of both series of hybrid hydrogels, it becomes apparent that the signal intensities are markedly influenced by the concentration of encapsulated nanomaterial.

To investigate the interaction of the carbon surface with the hydrogel components, a comparison between the pristine carbon nanomaterials and those incorporated into the hydrogel matrix was conducted through the measurement of the corresponding Raman spectra. In the case of G4-GO-5 hydrogel, an upshift of approximately 20 cm^{-1} for the G band, compared to pristine GO, was observed (Figure S2a). Additionally, the intensity ratio of the D and G peaks (I_D/I_G) increased from 0.70 to 0.82 suggesting an increase in defects and indicating the interaction of GO with components of the hydrogel matrix also observed in previously reported studies between cyclodextrins and GO surface.[60]

The variations in the tangential displacement mode region of the Raman spectra in the case of the G4-CNT-5 hydrogel in comparison to pristine SWNTs are highlighted in Figure S2b. The graphite-like G mode in the G4-CNT-5 sample exhibits an upward shift of approximately 8 cm^{-1} after the dispersion of nanotubes in the hydrogel matrix. This observed upshift in the G4-CNT-5 hydrogel may stem from strains induced by the adsorption of hydrogel constituents on the surface of the nanotubes, particularly cyclodextrins and G4s. Comparable G-band peaks shift values have been previously reported in

https://doi.org/10.1021/acsomega.3c07724
ACS Omega 2024, 9, 15833−15844

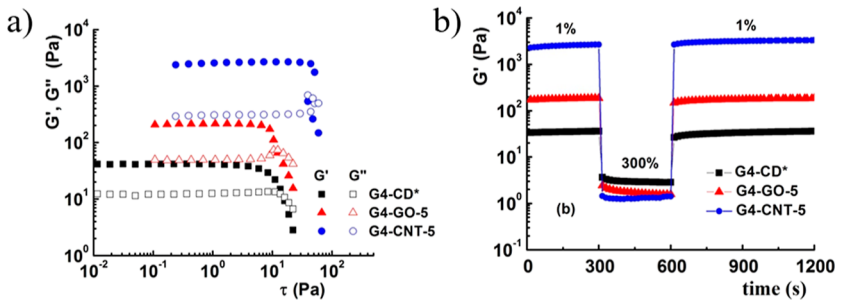

Figure 2. Rheological behavior of **G4-CD***,[45] **G4-GO-5,** and **G4-CNT-5** samples at 25 °C; (a) viscoelastic moduli, G' and G'', as a function of applied shear stress (τ) at 10 rad/s and (b) variation of G' with strain alternation from 1 to 300% at a constant frequency of 10 rad/s.

pristine SWNTs when compared to SWNT/γ-cyclodextrin composites,[56] SWNT/substituted β-CD,[61,62] or SWNT/ β-CD polymer[63] systems, and were explained by either hydrophobic interactions with the polymer[63] or multiple van der Waals attraction forces between CD and the carbon nanomaterial.

To further assess the incorporation of carbon nanomaterials and their impact on the physical properties of the resulted composite materials, rheological investigations were conducted on the hydrogel samples with the maximum amount of nanomaterials. All the examined samples exhibited solid-like behavior, as evidenced by the elastic modulus (G') being higher than the viscous modulus (G'') (Figure 2).

The obtained data revealed the fact that viscoelastic parameters exhibited a noticeable increase in the following order: G4-CD < G4-GO-5 < G4-CNT-5. Notably, the G4-CNT-5 sample manifested the strongest network, reflected in its highest G' and G'' values (G' = 2630 Pa and G'' = 325 Pa at an oscillation frequency of 10 rad/s and a shear stress of 1 Pa). For the G4-CNT-5 sample, G' and G'' are 1 and 2 orders of magnitude larger than those for G4-GO-5 and G4-CD, respectively. The loss tangent (tan δ), representing the ratio of viscous and elastic moduli (G''/G'), provides insights into the viscoelasticity of the samples under investigation. A lower tan δ value corresponds to a higher elastic modulus. Consequently, the G4-CNT-5 sample demonstrates the lowest tan δ value at 10 rad/s and 1 Pa (0.12) in comparison to G4-GO-5 (0.23) and G4-CD (0.30). This outcome reflects an enhanced elasticity due to the incorporation of carbon nanotubes. Both G' and G'' values remained constant up to a limiting shear stress, beyond which the hydrogel structure underwent changes. The G4-CNT-5 sample showed the widest viscoelastic linear range, wherein G' and G'' were unaffected by the applied shear stress. This stability persisted up to around 30 Pa, while the sample with GO maintained stability below approximately 7 Pa. It is noteworthy that the incorporation of GO did not alter the viscoelastic linear range compared to G4-CD.

The structure recovery test involved a continuous measurement of rheological parameters, alternating the strain from 1% (300 s) to 300% (300 s), followed by monitoring the recovery for 600 s. As depicted in Figure 2b, the elastic moduli remained constant under 1% strain, maintaining the same order observed in amplitude sweep measurements (G4-CD < G4-GO-5 < G4-CNT-5). Upon the application of high strain for 300 s, G' instantaneously decreased. However, following the removal of this high strain pulse, the internal network of hydrogels containing carbon nanotubes and GO completely recovered (100%) within 600 s, in contrast to G4-CD samples, which achieved up to 93.46% recovery from their initial structure. The incorporation of carbon nanotubes and GO significantly contributed to the enhancement of the recovery degree.

The difference regarding the resulting internal structure of the two composite series, determined by the different interactions of the β-CD network with GO, respectively, SWNTs, was also investigated via CD spectroscopy. The samples were extracted directly from the settled reaction mixture, and their measurements were conducted at 25 °C within a wavelength range of 220−340 nm (Figures S3 and S4). For all G4-GO_1−5 formulations, two distinct bands were identified: a negative peak at approximately 260 nm and a positive peak around 300 nm. The negative band is characteristic to guanosine analogue assemblies, which form distinct G4 structural units.[64,65] Notably, with an increasing concentration of GO within the hydrogel matrix, there was a clear enhancement in the band intensity at 260 nm. This observation suggests that the GO plays a pivotal role in stabilizing both the G4 assemblies and, consequently, the overall hydrogel structures. The positive band at 300 nm was attributed to β-CD stacking guided by G4 units, leading to the formation of cyclodextrin-guanosine fibrils or wires.[45] Interestingly, this band decreases considerably in intensity (completely disappearing in G4-GO-4 and G4-GO-5, Figure S3) with the increase in the GO concentration. We hypothesize that the extensive surface area of GO promotes two key phenomena: first, it aids in stabilizing the G4 structures, as evidenced by the increase in the negative 260 nm band and second, it facilitates the interaction between individual β-CD molecules and the GO surface through extensive hydrogen bonding, a process that ultimately disrupts the stacking of β-CD molecules.

In the context of formulations involving SWNTs, two distinct negative bands were observed: one at 260 nm, indicating the presence of assembled G4 units, and another around 300 nm, which signifies the self-assembly of β-CD molecules (Figure S4). Interestingly, the intensities of these bands exhibited a direct correlation with the concentration of the encapsulated SWNTs. This suggests that the binding of β-CD molecules along the cylindrical carbon nanotubes facilitates a β-CD molecular self-assembly, even at high concentrations of SWNTs.

The presence of G4 units within the composite's structure, as observed during CD analysis, was further confirmed through powder X-ray diffraction (PXRD) investigations (Figures S5 and S6). The PXRD patterns of G4-GO_1−5 xerogels revealed distinct features: a broad and faint diffraction peak centered at 2θ = 18.8°, indicating a layer distance (d) of 4.7 Å that is characteristic of channel-type assemblies formed by the alignment and stacking of β-CD molecules.[45] Additionally, another peak at 26.5° was observed, representing the $\pi-\pi$

https://doi.org/10.1021/acsomega.3c07724
ACS Omega 2024, 9, 15833−15844

distance between G-quartet stacks and corresponding to an intramolecular *d*-spacing of 3.4 Å.[40,65] In the context of SWNT xerogels, it is noteworthy that two prominent reflections (at 18.8 and 26.8°) can be identified and associated with intermolecular *d*-spacing values of 3.3 and 4.7 Å, respectively.

To further investigate the impact of nanomaterials on the properties of the composites, we conducted an evaluation of formulations G4-CNT_1−5 and G4-GO_1−5, focusing on their water retention characteristics (Figures S7 and S8). Regarding the CNT hydrogels, the observations revealed their respective maximum water retention volumes as follows: G4-CNT-1 (7 mL), G4-CNT-2 (8 mL), G4-CNT-3 (8 mL), G4-CNT-4 (10 mL), and G4-CNT-5 (11 mL). In the case of the GO formulations, the determined maximum water retention volumes were as follows: G4-GO-1 (5 mL), G4-GO-2 (6 mL), G4-GO-3 (6 mL), G4-GO-4 (7 mL), and G4-GO-5 (7 mL). Upon analyzing these results, it becomes evident that the water retention capacity is influenced by both the type of encapsulated nanomaterial and its corresponding concentration. Notably, SWNT-based formulations exhibit superior water retention characteristics compared to GO-based formulations. This observation can be attributed to the distinct assembly mechanisms exhibited by the nanomaterials in conjunction with the other components of the hydrogel (G4 and β-CD stacking).

We next conducted the SEM analysis on lyophilized samples of both G4-GO_1−5 and G4-CNT_1−5 hydrogels to investigate their morphology (Figures 3, S9 and S10) and compared them with the initial G4-CD.[45] The examined SEM images revealed that the cross-sectional morphology and porosity of the hydrogel network were notably affected by the type and amount of nanomaterial present in the sample.

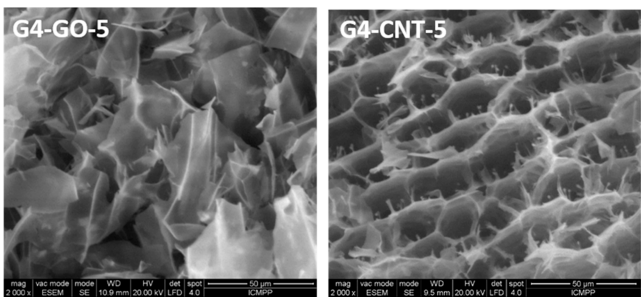

Figure 3. Representative SEM images of freeze-dried G4-GO-5 (left) and G4-CNT-5 (right) hydrogels.

The G4-CNT_1−5 xerogels exhibited well-organized structures with pores of varying dimensions [Figures 3 (right) and S9], resembling the structure of the reported G4-CD but with a slight tendency toward deformation of pores observed in G4-CNT-5 (Figure 3, right), which contains the highest amount of SWNTs. In the case of G4-GO_1−5, the deformation of the pore shapes and sizes was noticeable already for G4-GO-2 (Figure S10), leading to disordered arrangements without visible pores in the case of G4-GO-5 (Figure 3, left).

An additional experiment was performed on the xerogels to assess their stability over time. Fourier transform infrared (FTIR) spectra for G4-GO-5 (Figure S11, left) and G4-CNT-5 xerogels (Figure S11, right) were measured immediately postlyophilization (t = 0) and again after a 15-day period. Analyzing the characteristic peaks corresponding to β-CD molecules, boronic ester moieties, or guanosine, no shifts in the absorption bands were observed between t = 0 and t = 15 days, signifying the stability of the xerogels over this time interval.

2.2. Related Photothermal Properties. Both SWNTs[66,67] and GO[68,69] emerge as promising candidates for photothermal therapeutic agents, as they generate substantial amounts of heat when excited with near-infrared (IR) light (700−1100 nm). Notably, near-IR (NIR) light is transparent to biological systems, including skin, making these materials well-suited for photothermal applications. To explore the photothermal characteristics of composite hydrogels, we monitored the temperature increase induced by irradiation with a 1064 nm laser. Thermal imaging using an IR camera was employed to capture the temperature changes in composite samples enriched with the maximum content of carbon nanomaterials, as depicted in Figure 4.

Furthermore, cyclic heating tests specifically for these samples were conducted, demonstrating the remarkable photothermal stability of the hydrogels, as illustrated in Figure 5.

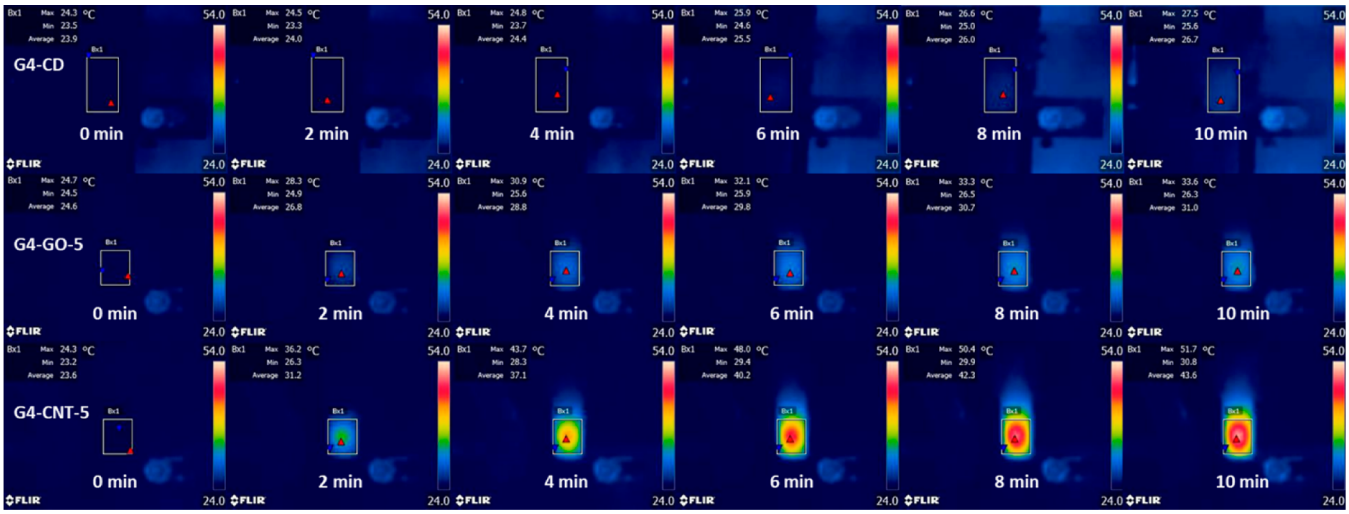

Figure 4. Thermal images recorded by an IR camera (FLIR C2) during 1064 nm laser irradiation (power density of 2 W/cm^2) of a PMMA cuvette containing 500 μL of **G4-CD**, **G4-GO-5**, and **G4-CNT-5** hydrogels.

https://doi.org/10.1021/acsomega.3c07724
ACS Omega 2024, 9, 15833−15844

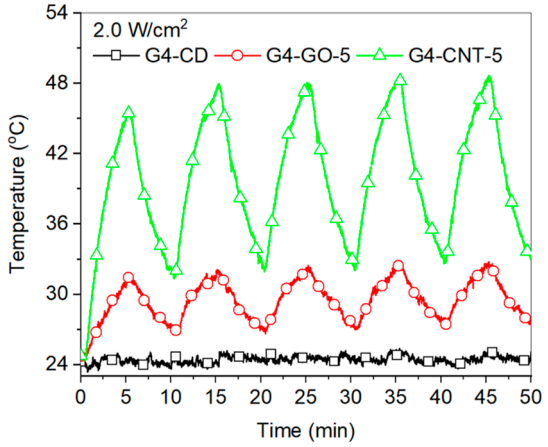

Figure 5. Photostability of the **G4-CD**, **G4-GO-5**, and **G4-CNT-5** hydrogels over 5 laser heating (2.0 W/cm^2) and natural cooling cycles.

The photothermal properties of all G4-GO_1−5, G4-CNT_1−5 samples, and free hydrogels as the control were evaluated in the presence of NIR laser irradiation at 1064 nm (Figures 6 and S12). Notably, we observed that both the type

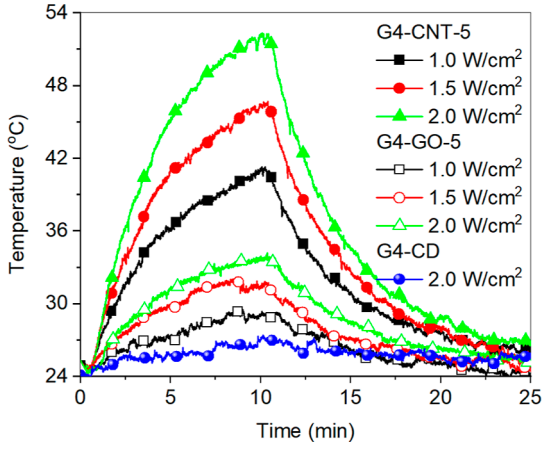

Figure 6. Temperature variation curves using different power densities (1.0, 1.5, and 2.0 W/cm^2) for the **G4-GO-5**, **G4-CNT-5**, and **G4-CD** samples (hydrogel without carbon nanomaterials) irradiated for 10 min.

of nanomaterial used (whether GO or SWNTs) and the concentration at which it was encapsulated significantly influenced the intensity of the temperature increase. Specifically, hydrogels based on SWNTs, when encapsulated at their maximum concentration, exhibited superior photothermal properties, reaching a temperature of 52 °C. In contrast, hydrogels based on GO, even at their maximum concentration, reached a lower temperature of 34 °C under the same conditions.

The less pronounced temperature rise observed in the case of the GO hydrogel can be attributed to the suboptimal absorption of NIR light by GO in its highly oxidized state.[70,71] This observation is also supported by the results of Markovic et al.,[72] who conducted a comparison between nonoxidized graphene and SWNTs under identical conditions of NIR irradiation. Graphene exhibited greater heat generation than SWNTs under the same experimental conditions.

Analyzing temperature variations of the composite samples induced by laser irradiation at 1064 nm (Figure S13), we further investigated the antimicrobial activity against *S. aureus* cultures of the selected G4-GO-5 and G4-CNT-5 hydrogels under similar NIR irradiation conditions.

2.3. In Vitro Antibacterial Activity. In our previous investigation, we evaluated the antimicrobial efficacy of the G4-CD hydrogel against eight distinct reference strains. These included bacterial strains, such as *S. aureus*, *Escherichia coli*, *Enterococcus faecalis*, *Klebsiella pneumoniae*, and *Salmonella typhimurium*, as well as yeast strains represented by *Candida albicans* and *Candida glabrata*. Additionally, the fungal strain, *Aspergillus brasiliensis*, was included in the evaluation. The obtained results revealed that the hydrogel exhibited only selective antimicrobial activity against *S. aureus*, with no significant impact on the other tested strains. In the current study, the antibacterial activity of the selected composite hydrogels against *S. aureus* was assessed by counting viable bacterial cells in contact with the samples with and without NIR irradiation. Remarkably, all samples exhibited significant antibacterial properties within just 10 min of exposure. Specifically, the G4-CNT-5 samples were particularly effective, reducing *S. aureus* cell counts by over 65% without NIR irradiation and achieving an even higher reduction of up to 86% with NIR irradiation (Figures 7 and 8). Similarly, the G4-

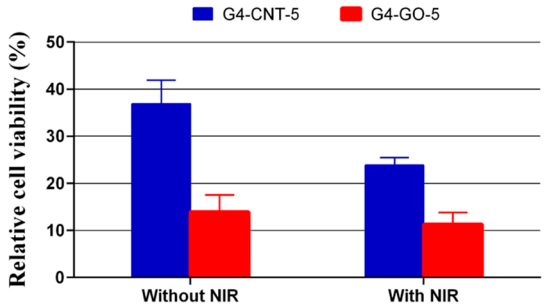

Figure 7. Antibacterial activity of the G4-CNT-5 and G4-GO-5 hydrogels against *S. aureus* before and after NIR irradiation (n = 3, error bars indicate standard deviation).

GO-5 samples exhibited substantial antibacterial activity, reducing bacterial populations by up to 76% without NIR irradiation and achieving an 88% reduction after NIR exposure. Notably, NIR irradiation enhanced the antimicrobial activity of both sample types. In the case of G4-CNT-5, the sample became more efficient after NIR irradiation, exhibiting a 13% improvement. On the contrary, for G4-GO-5, the enhancement was more modest but still notable, with a 2% increase in efficiency after NIR irradiation.

The enhanced antibacterial effectiveness observed in the hydrogel containing GO can be attributed to various mechanisms, including the induction of oxidative stress, either with or without the production of reactive oxygen species.[73] Additionally, due to the high surface area, it could be attributed to the wrapping of the bacterial cell membrane, which obstructs membrane transport. Another possibility is that the sharp edges of the GO nanosheets act as nanoknives, thereby cutting through the cell membrane's edges. This action induces cellular envelope stress and ultimately leading to bacterial inactivation through the leakage of intracellular content.[74−80]

On the contrary, the primary toxicity mechanism of SWNTs lies in their direct contact and subsequent damage to cells.

https://doi.org/10.1021/acsomega.3c07724
ACS Omega 2024, 9, 15833−15844

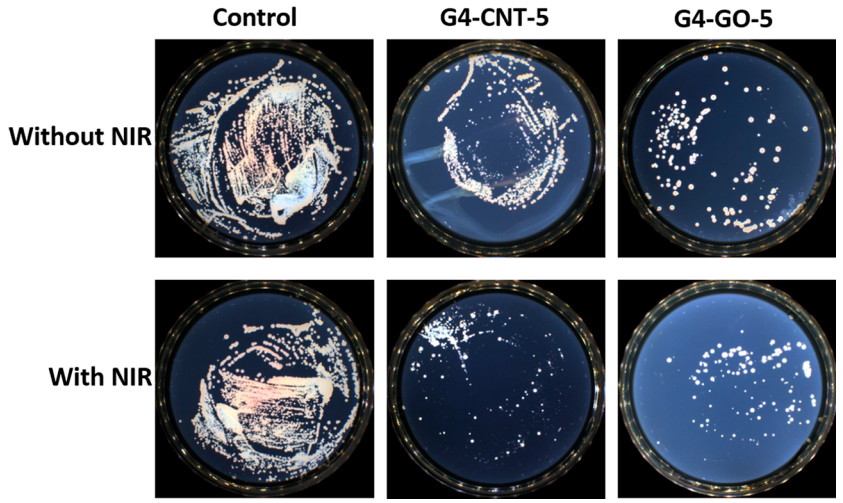

Figure 8. Growth inhibition of the bacterial colonies on PCA plates without and with NIR compared with control samples.

Consequently, the diameter of CNTs becomes a critical factor influencing the deactivation of microbial cells.[81−84] Moreover, β-CD molecules possess the capability to disrupt bacterial membranes, which leads to the efflux of K^+ ions from the bacterial membrane[45,46] thus enhancing the antimicrobial activity of both hydrogels under investigation.

The enhanced antibacterial properties exhibited by the examined composite hydrogels under NIR irradiation are attributed mostly to the thermal effect. This effect induced the disruption of physical bonds within the supramolecular hydrogel matrix, consequently facilitating the release of both hydrogel components and nanomaterials. This increased release exposes the hydrogel components to a greater surface area, enhancing their contact with the target bacteria and contributing to an overall antimicrobial effect.

The systems presented above offer a promising strategy for addressing *S. aureus* infections, providing a possible solution to combat antibacterial resistance that arises from traditional antibiotic-based treatments. In contrast to conventional approaches relying on antimicrobial agents, which can contribute to antibiotic resistance over time, particularly with multidrug-resistant organisms, photothermal hydrogels leverage light-responsive materials to generate localized heat, resulting in heightened antibacterial activity. Upon a review of recent literature, we have observed the emergence of systems demonstrating efficacy against *S. aureus*, in some cases comparable to those proposed by us, utilizing GO[85−88] and carbon nanotubes.[36,58,89]

2.4. In Vitro Biocompatibility. The investigation of cytotoxicity involved subjecting G4-CD, G4-GO-5, and G4-CNT-5 hydrogels to human gingival fibroblasts (HGF cells) using the MTS cell proliferation assay (Figure 9). Cell viability, expressed as a percentage relative to untreated cells supported by the culture medium, was calculated. The composite hydrogels were evaluated at the maximum concentration of carbon nanomaterial (0.5 mg/mL) to assess their highest impact on cell viability. The results, derived from three independent MTS tests with a minimum of six replicates for each hydrogel type, revealed mild cytotoxicity (above 60%)[90] for the hydrogel samples after 24 h. Notably, G4-CNT-5 exhibited slightly higher cell viability (78%), while G4-GO-5 displayed lower viability (62%) compared to the original G4-CD hydrogel (67%).

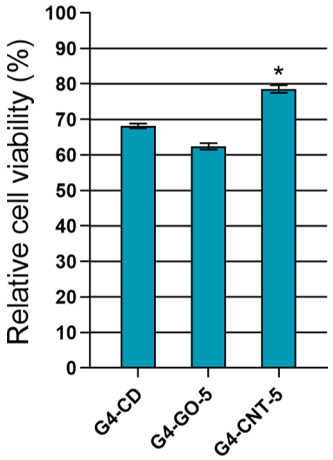

Figure 9. Results of biocompatibility of **G4-CD**, **G4-GO-5**, and **G4-CNT-5** hydrogels with the MTS assay. Data are presented as means ± S. D. (standard deviation), $n = 3$; *$p < 0.05$ (G4-GO-5 vs G4-CNT-5).

The cytotoxicity data acquired through this study provide a foundation for asserting a positive cytotoxic profile for the examined composite materials and indicate that these composite materials exhibit minimal adverse effects on cellular health.

3. CONCLUSIONS

We have successfully synthesized two distinct series of composite hydrogels by integrating them into G4-based hydrogels, enriched with β-CD, of two different carbon nanomaterials: GO and SWNTs. Our investigation focused on elucidating the composite hydrogel network, with particular attention given to the interactions between β-CD and GO as well as SWNTs. To evaluate the photothermal properties of these composite materials, the samples were subjected to NIR laser irradiation at 1064 nm. Our observations revealed that both the choice of nanomaterial (GO or SWNTs), and its concentration within the hydrogel matrix significantly influenced the intensity of the temperature increase. Hydrogels incorporating SWNTs, at their maximum concentration, exhibited superior photothermal properties, achieving a remarkable temperature increase of up to 52 °C. In contrast,

https://doi.org/10.1021/acsomega.3c07724
ACS Omega 2024, 9, 15833−15844

hydrogels containing GO, even at their maximum concentration, reached a comparatively lower temperature of 34 °C under identical conditions. Furthermore, when these composite hydrogels were fully loaded with carbon nanomaterials, they exhibited synergistically enhanced antibacterial activity against *S. aureus*. This outcome highlights the potential of these systems as a notable antimicrobial platform, which benefits from the synergistic interplay between the gel matrix, carbon nanomaterials, and the photothermal effects. Additionally, the presence of covalently bound cyclodextrin in these designed systems opens up exciting possibilities for loading water-insoluble antibiotics, making these systems a versatile platform for future therapeutic applications.

4. MATERIALS AND METHODS

4.1. Materials. The chemicals utilized in this study, including guanosine, LiOH·H_2O, KOH, and SWNTs (0.7−1.1 nm diameter), were purchased from Sigma (Schnelldorf, Germany). β-CD, benzene-1,4-diboronic acid, and GO (10 mg/mL, dispersed in water) were procured from TCI (Tokyo, Japan). All purchased reagents were utilized without additional purification. Ultrapure water was used throughout the experimental procedures and for preparing stock solutions.

4.2. Synthesis of SWNT Composite Hydrogels (G4-CNT_1−5). Composite hydrogels G4-CNT_1−5 were prepared utilizing an adapted synthetic protocol.[48] First, in a glass vial, a SWNT stock solution was prepared by mixing 88.1 mM 1,4-benzene diboronic acid (116.8 mg), 12.6 mM β-CD (1012 μL of stock solution containing 0.565 g of β-CD in 5 mL of water), 176.4 mM LiOH (800 μL of stock solution containing 0.148 g of LiOH·H_2O in 2 mL of water), and 6188 μL of water. The resultant mixture underwent a 2 min sonication process, followed by heating on an oil bath at 110 °C until it transformed into a clear, transparent solution. Next, an amount of 88.3 mM of guanosine (0.2 g) was added and the mixture heated on an oil bath at 110 °C until the entire guanosine is dissolved. After cooling down to room temperature, 4 mg of SWNTs were added to the transparent reaction mixture, and the suspension sonicated for 1 h to afford 8 mL of stable black suspension of SWNT (0.5 mg/mL).

Separately, the β-CD hydrogel matrix was prepared by mixing in a glass vial 44 mM 1,4-benzene diboronic acid (29.2 mg), 6.3 mM β-CD (253 μL of stock solution containing 0.565 g of β-CD in 5 mL of water), 88 mM KOH (200 μL of stock solution containing 0.488 g of KOH in 5 mL of water), and water. The resultant mixture underwent a 2 min sonication process, followed by heating on an oil bath at 110 °C until it transformed into a clear transparent solution. Next, an amount of 44.1 mM of guanosine (50 mg) was added and the mixture heated on an oil bath at 110 °C until the entire guanosine is dissolved.

Five composite hydrogels (G4-CNT_1−5) were synthesized by combining various amounts of the above prepared SWNT stock solution (200, 600, 1000, 1400, 2000 μL, containing 0.1, 0.3, 0.5, 0.7, and 1 mg of CNTs, respectively) and β-CD hydrogel (Table S1).

4.3. Synthesis of GO Composite Hydrogels (G4-GO_1−5). The β-CD hydrogel matrix was prepared following the same procedure as described in 2.2. Five GO composite hydrogels (G4-GO_1−5) were synthesized by adding different volumes (10, 30, 50, 70, and 100 μL, containing 0.1, 0.3, 0.5, 0.7, and 1 mg) of commercial GO solution (10 mg/mL) with the β-CD hydrogel matrix (Table S1).

4.4. Characterization of Hydrogels. A water retention experiment was conducted for all of the obtained hydrogel samples. Each sample underwent successive additions of 1 mL of water with stirring to the initial sample volume (4 mL) until maximum water retention was achieved. Subsequently, after the relaxation time (24 h), the self-sustainability of each sample was assessed by inverting the sample vial.

Rheological measurements were conducted at a temperature of 25 °C using an MCR302 Anton-Paar rheometer, employing plane−plane geometry with a 25 mm diameter and an antievaporation device. The viscoelastic properties of the two samples, featuring the highest concentrations of carbon nanotubes and GO, were determined through amplitude sweep and oscillatory step tests. Amplitude sweep tests were performed at a frequency of 10 rad/s within a stress range of 10^{-2} to 10^{2} Pa to establish the linear viscoelastic domain for each sample. Oscillatory step tests, conducted at 10 rad/s, alternated between 300 s at a low strain (1%) and 300 s at a high strain (300%), with the subsequent monitoring of structure recovery over a duration of 600 s.

CD measurements were carried out using a Chirascan plus instrument (Applied Photophysics Ltd., Leatherhead, Surrey, UK). CD spectra were recorded within the range of 340−220 nm, with data pitch 0.5 at 200 nm·min^{-1} acquisition speed. Measurements were performed in 1 mm lamellas. Typically, 100 μL of the reaction mixture sample (prepared at 25 °C) was directly applied onto a lamella covered with another glass slide, ensuring the formation of a uniform film.

Raman spectra for composite hydrogels were recorded using an inVila Raman confocal microscope (Renishaw, New Mills, UK) outfitted with a He−Ne laser (at 442 nm for GO and 633 nm for SWNTs) and a RenCam CCD detector linked to a Leica 2500 M microscope. All measurements were conducted in a backscattering configuration employing a 50× objective at room temperature and atmospheric pressure.

The morphology of the hydrogels was examined by SEM. The analyses were carried out using an FEI NanoSEM430 (Hillsboro, USA). Prior to measurements, hydrogel samples were freeze-dried, carefully positioned onto 25 aluminum plates with double-sided adhesive, and examined at an acceleration voltage of 20 kV.

X-ray diffraction analysis was conducted using a Rigaku Miniflex 600 diffractometer (Rigaku, Tokyo, Japan), using Cu Kα emission within the angular range of 2−50° (2θ). The scanning step was set at 0.01°, and data was recorded at a rate of 2°/min.

The FTIR spectra of G4-GO-5 and G4-CNT-5 xerogels were recorded by the ATR technique using INVENIO-R FTIR spectrometer (Bruker, Ettingen, Germany), with 90 scans at a resolution of 4 and in the spectral range 4000−400 cm^{-1}. FTIR spectra were processed using OPUS 8.7.41 and OriginPro 8 software.

4.5. Photothermal Effect of Composite Hydrogels. Volumes of 500 μL of investigated hydrogel composites were placed in 1.5 mL PMMA cuvettes and irradiated using a 1064 nm NIR laser for a duration of 10 min, with a laser density set at 2 W/cm^2. For samples G4-CNT-5 and G4-GO-5, two additional irradiation powers were applied, specifically 1 and 1.5 W/cm^2, respectively.

4.6. Evaluation of Antibacterial Activity in Vitro. The antimicrobial activity screening of the hydrogel samples before and after irradiation was performed by using viable cell-counting method.[91] The bacterial strain *S. aureus* ATCC25923

https://doi.org/10.1021/acsomega.3c07724
ACS Omega 2024, 9, 15833−15844

(*S. aureus*) was refreshed on an nutrient agar at 37 °C. A microbial suspension was prepared with this culture in sterile distilled water to obtain turbidity optically comparable to that of 0.5 McFarland standards. 100 μL of bacterial suspensions (0.5 McFerland) were added on 500 μL hydrogels, and irradiated with an NIR laser (1064 nm; laser density 2 W/cm^2) for 10 min. Nutrient broth medium (1 mL) was added, and the hydrogels were incubated for 24 h. A control experiment was also conducted. Five microliters of the control samples and of the irradiated samples were removed and spread on plate count agar (PCA) plates. The number of colonies was counted after 24 h of incubation at 37 °C. All tests were carried out in triplicate to verify the results. After incubation, the plates were analyzed with SCAN1200, version 8.6.10.0 (Interscience, France) and the number of colonies was expressed as the mean ± standard deviation performed with GraphPad Prism software version 9.5.1 for Windows (GraphPad Software, La Jolla California USA, www.graphpad.com). The ratio of inhibited growth of bacteria (IRG) was calculated, which is defined as

$$\mathrm{IRG}(\%) = ((\mathrm{Na} - \mathrm{Nb}))/\mathrm{Na} \times 100\%$$

where: Na and Nb are the average values of colonies of the control group and the experimental groups, respectively.

4.7. Biocompatibility (MTS Assay). The biocompatibility of **G4-CD**, **G4-GO-5**, and **G4-CNT-5** hydrogels was evaluated by the MTS assay using the CellTiter 96 AQueous One Solution Cell Proliferation Assay from Promega, according to the manufacturer's instructions and based on the direct contact procedure from the international standard ISO 10993−5:2009(E). Human gingival fibroblasts (HGF cells) were grown in Alpha MEM Eagle completed with a 10% fetal bovine serum (FBS) and 1% mixture of antibiotic-antimycotic in a humidified atmosphere with 5% CO_2 at 37 °C. The cells were maintained in culture dishes until they reached subconfluency. In order to prepare the test samples for this assay, they were immersed in a complete culture medium in a 24-well plate. After 24 h of incubation in a humidified atmosphere with 5% CO_2 at 37 °C, the medium was discarded and the HGF cells were seeded over the samples, at a density of 5×10^4 cells/mL in 0.5 mL cell culture medium/well. The control group was represented by untreated cells. The plates were placed in the cell culture incubator and, after 24 h, a MTS reagent was added. After the formazan formation, the solutions were transferred into a 96-well plate and then, on a FLUOstar Omega microplate reader from BMG LABTECH, the optical density was measured at 490 nm. The experiments were done in triplicate and treated cell viability was expressed as a percentage of untreated cells' viability. Graphical data were expressed as means ± standard deviation (S. D.). The statistical analysis was made in GraphPad Prism 8 with One-way ANOVA using Dunn's multiple comparison test. The differences were considered statistically different when $p < 0.05$.

■ ASSOCIATED CONTENT

Supporting Information

The Supporting Information is available free of charge at https://pubs.acs.org/doi/10.1021/acsomega.3c07724.

Composition of hydrogels, Raman spectra, CD spectra, PXRDs, water retention properties, SEM images, FTIR spectroscopy, and photothermal properties (PDF)

■ AUTHOR INFORMATION

Corresponding Author

Alexandru Rotaru − *"Petru Poni" Institute of Macromolecular Chemistry, Romanian Academy, Centre of Advanced Research in Bionanoconjugates and Biopolymers, 700487 Iasi, Romania;* orcid.org/0000-0002-1280-9515; Email: rotaru.alexandru@icmpp.ro

Authors

Monica-Cornelia Sardaru − *The Research Institute of the University of Bucharest (ICUB), 050663 Bucharest, Romania; "Petru Poni" Institute of Macromolecular Chemistry, Romanian Academy, Centre of Advanced Research in Bionanoconjugates and Biopolymers, 700487 Iasi, Romania*

Irina Rosca − *"Petru Poni" Institute of Macromolecular Chemistry, Romanian Academy, Centre of Advanced Research in Bionanoconjugates and Biopolymers, 700487 Iasi, Romania;* orcid.org/0000-0003-3080-1709

Cristian Ursu − *"Petru Poni" Institute of Macromolecular Chemistry, Romanian Academy, Physics of Polymers and Polymeric Materials Laboratory, 700487 Iasi, Romania*

Ioan-Andrei Dascalu − *"Petru Poni" Institute of Macromolecular Chemistry, Romanian Academy, Centre of Advanced Research in Bionanoconjugates and Biopolymers, 700487 Iasi, Romania;* orcid.org/0000-0002-0715-6855

Elena-Laura Ursu − *"Petru Poni" Institute of Macromolecular Chemistry, Romanian Academy, Centre of Advanced Research in Bionanoconjugates and Biopolymers, 700487 Iasi, Romania*

Simona Morariu − *Natural Polymers, Bioactive and Biocompatible Materials, "Petru Poni" Institute of Macromolecular Chemistry, Romanian Academy, Iasi 700487, Romania*

Complete contact information is available at: https://pubs.acs.org/10.1021/acsomega.3c07724

Author Contributions

Conceptualization, M.-C.S. and A.R.; methodology, M.-C.S. and A.R.; validation, M.-C.S., I.R., E.-L.U., and A.R.; formal analysis, M.-C.S., C.U., I.-A.D., I.R., S.M., and E.-L.U. investigation, M.-C.S., C.U., I.-A.D., I.R., and E.-L.U.; data curation, M.-C.S. and A.R.; writing—original draft preparation, M.-C.S. and A.R.; and writing—review and editing, M.-C.S., C.U., I.R., S.M., and A.R. All authors have read and agreed to the published version of the manuscript.

Notes

The authors declare no competing financial interest.

■ ACKNOWLEDGMENTS

We acknowledge the support provided by the ICUB Fellowship for Young Researchers (M.C.S., Contract no. 26172/29 November 2022). This project has received funding from the H2020-MSCA-RISE-2019 under grant agreement no. 872331 (acronym: NoBiasFluors).

■ REFERENCES

(1) Liu, J.; Wu, D.; Zhu, N.; Wu, Y.; Li, G. Antibacterial Mechanisms and Applications of Metal-Organic Frameworks and Their Derived Nanomaterials. *Trends Food Sci. Technol.* **2021**, *109*, 413−434.

(2) Ma, T.; Huang, K.; Cheng, N. Recent Advances in Nanozyme-Mediated Strategies for Pathogen Detection and Control. *Int. J. Mol. Sci.* **2023**, *24* (17), 13342.

(3) Moghadam, M. T.; Khoshbayan, A.; Chegini, Z.; Farahani, I.; Shariati, A. Bacteriophages, a New Therapeutic Solution for Inhibiting Multidrug-Resistant Bacteria Causing Wound Infection: Lesson from Animal Models and Clinical Trials. *Drug Des., Dev. Ther.* **2020**, *14*, 1867−1883.
(4) Andersson, D. I.; Hughes, D. Antibiotic Resistance and Its Cost: Is It Possible to Reverse Resistance? *Nat. Rev. Microbiol.* **2010**, *8* (4), 260−271.
(5) van Hoek, A.; Mevius, D.; Guerra, B.; Mullany, P.; Roberts, A.; Aarts, H. Acquired Antibiotic Resistance Genes: An Overview. *Front. Microbiol.* **2011**, *2*, 12596.
(6) Blair, J. M. A.; Webber, M. A.; Baylay, A. J.; Ogbolu, D. O.; Piddock, L. J. V. Molecular Mechanisms of Antibiotic Resistance. *Nat. Rev. Microbiol.* **2015**, *13* (1), 42−51.
(7) Durão, P.; Balbontín, R.; Gordo, I. Evolutionary Mechanisms Shaping the Maintenance of Antibiotic Resistance. *Trends Microbiol.* **2018**, *26* (8), 677−691.
(8) Jia, B.; Du, X.; Wang, W.; Qu, Y.; Liu, X.; Zhao, M.; Li, W.; Li, Y. Nanophysical Antimicrobial Strategies: A Rational Deployment of Nanomaterials and Physical Stimulations in Combating Bacterial Infections. *Adv. Sci.* **2022**, *9*, 2105252.
(9) Wang, Y.; Yang, Y.; Shi, Y.; Song, H.; Yu, C. Antibiotic-Free Antibacterial Strategies Enabled by Nanomaterials: Progress and Perspectives. *Adv. Mater.* **2020**, *32*, 1904106.
(10) He, T.; Lv, S.; Wei, D.; Feng, R.; Yang, J.; Yan, Y.; Liu, L.; Wu, L. Photothermal Conversion of Hydrogel-Based Biomaterial. *Chem. Rec.* **2023**, *23*, No. e202300184.
(11) Bai, G.; Yuan, P.; Cai, B.; Qiu, X.; Jin, R.; Liu, S.; Li, Y.; Chen, X. Stimuli-Responsive Scaffold for Breast Cancer Treatment Combining Accurate Photothermal Therapy and Adipose Tissue Regeneration. *Adv. Funct. Mater.* **2019**, *29*, 1904401.
(12) Gao, Q.; Zhang, X.; Yin, W.; Ma, D.; Xie, C.; Zheng, L.; Dong, X.; Mei, L.; Yu, J.; Wang, C.; Gu, Z.; Zhao, Y. Functionalized MoS2 Nanovehicle with Near-Infrared Laser-Mediated Nitric Oxide Release and Photothermal Activities for Advanced Bacteria-Infected Wound Therapy. *Small* **2018**, *14* (45), No. e1802290.
(13) Tan, L.; Li, J.; Liu, X.; Cui, Z.; X, Y.; Zhu, S.; Li, Z.; X, Y.; Yang, X.; Yeung, K. W. K.; Pan, H.; Wang, X.; Wu, S. Rapid Biofilm Eradication on Bone Implants Using Red Phosphorus and Near-Infrared Light. *Adv. Mater.* **2018**, *30* (31), 1801808.
(14) Ray, P. C.; Khan, S. A.; Singh, A. K.; Senapati, D.; Fan, Z. Nanomaterials for Targeted Detection and Photothermal Killing of Bacteria. *Chem. Soc. Rev.* **2012**, *41* (8), 3193−3209.
(15) He, W.; Wang, Z.; Bai, H.; Zhao, Z.; Kwok, R. T. K.; Lam, J. W. Y.; Tang, B. Z. Highly Efficient Photothermal Nanoparticles for the Rapid Eradication of Bacterial Biofilms. *Nanoscale* **2021**, *13* (32), 13610−13616.
(16) Vélez, D. G. G.; Álvarez, K. J. L.; Obando, M. P. R.; Vélez, D. G. G.; Álvarez, K. J. L.; Obando, M. P. R. Antibacterial Strategies: Photodynamic and Photothermal Treatments Based on Carbon-Based Materials. In *Biotechnology—Biosensors, Biomaterials and Tissue Engineering Annual*; IntechOpen, 2023; Vol. *2023*.
(17) Knoblauch, R.; Geddes, C. D. Carbon Nanodots in Photodynamic Antimicrobial Therapy: A Review. *Mater.* **2020**, *13* (18), 4004.
(18) Karnwal, A.; Kumar, G.; Pant, G.; Hossain, K.; Ahmad, A.; Alshammari, M. B. Perspectives on Usage of Functional Nanomaterials in Antimicrobial Therapy for Antibiotic-Resistant Bacterial Infections. *ACS Omega* **2023**, *8* (15), 13492−13508.
(19) Nanda, S. S.; Papaefthymiou, G. C.; Yi, D. K. Functionalization of Graphene Oxide and Its Biomedical Applications. *Crit. Rev. Solid State Mater. Sci.* **2015**, *40* (5), 291−315.
(20) Guo, X.; Gao, H.; Wang, S.; Yin, L.; Dai, Y. Scalable, Flexible and Reusable Graphene Oxide-Functionalized Electrospun Nanofibrous Membrane for Solar Photothermal Desalination. *Desalination* **2020**, *488*, 114535.
(21) Wang, X.; Zhu, L.; Gu, Z.; Dai, L. Carbon Nanomaterials for Phototherapy. *Nanophotonics* **2022**, *11* (22), 4955−4976.
(22) Liang, X.; Shang, W.; Chi, C.; Zeng, C.; Wang, K.; Fang, C.; Chen, Q.; Liu, H.; Fan, Y.; Tian, J. Dye-Conjugated Single-Walled Carbon Nanotubes Induce Photothermal Therapy under the Guidance of near-Infrared Imaging. *Cancer Lett.* **2016**, *383* (2), 243−249.
(23) Robinson, J. T.; Welsher, K.; Tabakman, S. M.; Sherlock, S. P.; Wang, H.; Luong, R.; Dai, H. High Performance In Vivo Near-IR (>1 Mm) Imaging and Photothermal Cancer Therapy with Carbon Nanotubes. *Nano Res.* **2010**, *3* (11), 779−793.
(24) Shih, C.-J.; Lin, S.; Sharma, R.; Strano, M. S.; Blankschtein, D. Understanding the pH-Dependent Behavior of Graphene Oxide Aqueous Solutions: A Comparative Experimental and Molecular Dynamics Simulation Study. *Langmuir* **2012**, *28* (1), 235−241.
(25) Ghulam, A. N.; Dos Santos, O. A. L.; Hazeem, L.; Backx, B. P.; Bououdina, M.; Bellucci, S. Graphene Oxide (GO) Materials-Applications and Toxicity on Living Organisms and Environment. *J. Funct. Biomater.* **2022**, *13* (2), 77.
(26) Cheng, C.; Li, S.; Thomas, A.; Kotov, N. A.; Haag, R. Functional Graphene Nanomaterials Based Architectures: Biointeractions, Fabrications, and Emerging Biological Applications. *Chem. Rev.* **2017**, *117* (3), 1826−1914.
(27) Reina, G.; González-Domínguez, J. M.; Criado, A.; Vázquez, E.; Bianco, A.; Prato, M. Promises, Facts and Challenges for Graphene in Biomedical Applications. *Chem. Soc. Rev.* **2017**, *46* (15), 4400−4416.
(28) Khan, M. U. A.; Stojanović, G. M.; Hassan, R.; Anand, T. J. S.; Al-Ejji, M.; Hasan, A. Role of Graphene Oxide in Bacterial Cellulose-Gelatin Hydrogels for Wound Dressing Applications. *ACS Omega* **2023**, *8* (18), 15909−15919.
(29) Anand, A.; Unnikrishnan, B.; Wei, S.-C.; Chou, C. P.; Zhang, L.-Z.; Huang, C.-C. Graphene Oxide and Carbon Dots as Broad-Spectrum Antimicrobial Agents - a Minireview. *Nanoscale Horiz.* **2019**, *4* (1), 117−137.
(30) Liu, S.; Zeng, T. H.; Hofmann, M.; Burcombe, E.; Wei, J.; Jiang, R.; Kong, J.; Chen, Y. Antibacterial Activity of Graphite, Graphite Oxide, Graphene Oxide, and Reduced Graphene Oxide: Membrane and Oxidative Stress. *ACS Nano* **2011**, *5* (9), 6971−6980.
(31) Yadav, N.; Dubey, A.; Shukla, S.; Saini, C. P.; Gupta, G.; Priyadarshini, R.; Lochab, B. Graphene Oxide-Coated Surface: Inhibition of Bacterial Biofilm Formation Due to Specific Surface-Interface Interactions. *ACS Omega* **2017**, *2* (7), 3070−3082.
(32) Bardhan, N. M.; Ghosh, D.; Belcher, A. M. Carbon Nanotubes as in Vivo Bacterial Probes. *Nat. Commun.* **2014**, *5* (1), 4918.
(33) Bekyarova, E.; Ni, Y.; Malarkey, E. B.; Montana, V.; McWilliams, J. L.; Haddon, R. C.; Parpura, V. Applications of Carbon Nanotubes in Biotechnology and Biomedicine. *J. Biomed. Nanotechnol.* **2005**, *1* (1), 3−17.
(34) Kang, S.; Pinault, M.; Pfefferle, L. D.; Elimelech, M. Single-Walled Carbon Nanotubes Exhibit Strong Antimicrobial Activity. *Langmuir* **2007**, *23* (17), 8670−8673.
(35) Patarroyo, J. L.; Cifuentes, J.; Muñoz, L. N.; Cruz, J. C.; Reyes, L. H. Novel Antibacterial Hydrogels Based on Gelatin/Polyvinyl-Alcohol and Graphene Oxide/Silver Nanoconjugates: Formulation, Characterization, and Preliminary Biocompatibility Evaluation. *Heliyon* **2022**, *8* (3), No. e09145.
(36) Patil, T. V.; Patel, D. K.; Dutta, S. D.; Ganguly, K.; Randhawa, A.; Lim, K.-T. Carbon Nanotubes-Based Hydrogels for Bacterial Eradiation and Wound-Healing Applications. *Appl. Sci.* **2021**, *11* (20), 9550.
(37) Tu, Y.; Chen, N.; Li, C.; Liu, H.; Zhu, R.; Chen, S.; Xiao, Q.; Liu, J.; Ramakrishna, S.; He, L. Advances in Injectable Self-Healing Biomedical Hydrogels. *Acta Biomater.* **2019**, *90*, 1−20.
(38) Kulkarni, N.; Rao, P.; Jadhav, G. S.; Kulkarni, B.; Kanakavalli, N.; Kirad, S.; Salunke, S.; Tanpure, V.; Sahu, B. Emerging Role of Injectable Dipeptide Hydrogels in Biomedical Applications. *ACS Omega* **2023**, *8* (4), 3551−3570.
(39) Lloyd, G. O.; Steed, J. W. Anion-Tuning of Supramolecular Gel Properties. *Nat. Chem.* **2009**, *1* (6), 437−442.
(40) Peters, G. M.; Skala, L. P.; Plank, T. N.; Hyman, B. J.; Manjunatha Reddy, G. N.; Marsh, A.; Brown, S. P.; Davis, J. T. A G_4·

https://doi.org/10.1021/acsomega.3c07724
ACS Omega 2024, 9, 15833−15844

K^+ Hydrogel Stabilized by an Anion. *J. Am. Chem. Soc.* **2014**, *136* (36), 12596−12599.
(41) Ghobril, C.; Grinstaff, M. W. The Chemistry and Engineering of Polymeric Hydrogel Adhesives for Wound Closure: A Tutorial. *Chem. Soc. Rev.* **2015**, *44* (7), 1820−1835.
(42) Yu, L.; Ding, J. Injectable Hydrogels as Unique Biomedical Materials. *Chem. Soc. Rev.* **2008**, *37* (8), 1473−1481.
(43) Sardaru, M.-C.; Morariu, S.; Carp, O.-E.; Ursu, E.-L.; Rotaru, A.; Barboiu, M. Dynameric G-Quadruplex-Dextran Hydrogels for Cell Growth Applications. *Chem. Commun.* **2023**, *59* (21), 3134−3137.
(44) Norahan, M. H.; Pedroza-González, S. C.; Sánchez-Salazar, M. G.; Álvarez, M. M.; de Santiago, G. T. Structural and Biological Engineering of 3D Hydrogels for Wound Healing. *Bioact. Mater.* **2023**, *24*, 197−235.
(45) Sardaru, M.-C.; Rosca, I.; Morariu, S.; Ursu, E.-L.; Ghiarasim, R.; Rotaru, A. Injectable Thixotropic β-Cyclodextrin-Functionalized Hydrogels Based on Guanosine Quartet Assembly. *Int. J. Mol. Sci.* **2021**, *22* (17), 9179.
(46) Yamamura, H.; Suzuki, K.; Uchibori, K.; Miyagawa, A.; Kawai, M.; Ohmizo, C.; Katsu, T. Mimicking an Antimicrobial Peptide Polymyxin B by Use of Cyclodextrin. *Chem. Commun.* **2012**, *48*, 892−894.
(47) Karginov, V. A.; Nestorovich, E. M.; Schmidtmann, F.; Robinson, T. M.; Yohannes, A.; Fahmi, N. E.; Bezrukov, S. M.; Hecht, S. M. Inhibition of S. aureus α-hemolysin and B. anthracis lethal toxin by β-cyclodextrin derivatives. *Bioorg. Med. Chem.* **2007**, *15* (16), 5424−5431.
(48) Ursu, E.-L.; Gavril, G.; Morariu, S.; Pinteala, M.; Barboiu, M.; Rotaru, A. Single-Walled Carbon Nanotubes-G-Quadruple Hydrogel Nanocomposite Matrixes for Cell Support Applications. *Mater. Sci. Eng., C* **2020**, *111*, 110800.
(49) Tang, Q.; Plank, T. N.; Zhu, T.; Yu, H.; Ge, Z.; Li, Q.; Li, L.; Davis, J. T.; Pei, H. Self-Assembly of Metallo-Nucleoside Hydrogels for Injectable Materials That Promote Wound Closure. *ACS Appl. Mater. Interfaces* **2019**, *11* (22), 19743−19750.
(50) Plank, T. N.; Skala, L. P.; Davis, J. T. Supramolecular Hydrogels for Environmental Remediation: G4-Quartet Gels That Selectively Absorb Anionic Dyes from Water. *Chem. Commun.* **2017**, *53* (46), 6235−6238.
(51) Rotaru, A.; Pricope, G.; Plank, T. N.; Clima, L.; Ursu, E. L.; Pinteala, M.; Davis, J. T.; Barboiu, M. G-Quartet Hydrogels for Effective Cell Growth Applications. *Chem. Commun.* **2017**, *53* (94), 12668−12671.
(52) Healy, B.; Yu, T.; da Silva Alves, D. C.; Okeke, C.; Breslin, C. B. Cyclodextrins as Supramolecular Recognition Systems: Applications in the Fabrication of Electrochemical Sensors. *Materials* **2021**, *14* (7), 1668.
(53) Zhong, Y.; He, Y.; Ge, Y.; Song, G. β-Cyclodextrin Protected Cu Nanoclusters as a Novel Fluorescence Sensor for Graphene Oxide in Environmental Water Samples. *Luminescence* **2017**, *32* (4), 596−601.
(54) Alam, A. U.; Qin, Y.; Catalano, M.; Wang, L.; Kim, M. J.; Howlader, M. M. R.; Hu, N. X.; Deen, M. J. Tailoring MWCNTs and β-Cyclodextrin for Sensitive Detection of Acetaminophen and Estrogen. *ACS Appl. Mater. Interfaces* **2018**, *10* (25), 21411−21427.
(55) Chen, J.; Dyer, M. J.; Yu, M.-F. Cyclodextrin-Mediated Soft Cutting of Single-Walled Carbon Nanotubes. *J. Am. Chem. Soc.* **2001**, *123* (25), 6201−6202.
(56) Chambers, G.; Carroll, C.; Farrell, G. F.; Dalton, A. B.; McNamara, M.; in het Panhuis, M.; Byrne, H. J. Characterization of the Interaction of Gamma Cyclodextrin with Single-Walled Carbon Nanotubes. *Nano Lett.* **2003**, *3* (6), 843−846.
(57) Huang, S.; Liu, H.; Liao, K.; Hu, Q.; Guo, R.; Deng, K. Functionalized GO Nanovehicles with Nitric Oxide Release and Photothermal Activity-Based Hydrogels for Bacteria-Infected Wound Healing. *ACS Appl. Mater. Interfaces* **2020**, *12* (26), 28952−28964.
(58) Du, G.; Nie, L.; Gao, G.; Sun, Y.; Hou, R.; Zhang, H.; Chen, T.; Fu, J. Tough and Biocompatible Hydrogels Based on in Situ Interpenetrating Networks of Dithiol-Connected Graphene Oxide and Poly(Vinyl Alcohol). *ACS Appl. Mater. Interfaces* **2015**, *7* (5), 3003−3008.
(59) López-Lorente, A. I.; Simonet, B. M.; Valcárcel, M. Raman Spectroscopic Characterization of Single Walled Carbon Nanotubes: Influence of the Sample Aggregation State. *Analyst* **2014**, *139* (1), 290−298.
(60) Nyairo, W. N.; Eker, Y. R.; Kowenje, C.; Zor, E.; Bingol, H.; Tor, A.; Ongeri, D. M. Efficient Removal of Lead(II) Ions from Aqueous Solutions Using Methyl-β-Cyclodextrin Modified Graphene Oxide. *Water Air Soil Pollut.* **2017**, *228* (11), 406.
(61) Bai, Y.; Xu, G. Y.; Sun, H. Y.; Hao, A. Y.; Mao, H. Z.; Dong, S. L.; Shi, X. F.; Xin, X.; Ao, M. Q.; Pang, J. Y.; Yang, X. D. Effect of Substituted Group of β-Cyclodextrin Derivatives on the Dispersing of Carbon Nanotubes. *J. Dispersion Sci. Technol.* **2010**, *31* (3), 353−358.
(62) Liu, K.; Fu, H.; Xie, Y.; Zhang, L.; Pan, K.; Zhou, W. Assembly of β-Cyclodextrins Acting as Molecular Bricks onto Multiwall Carbon Nanotubes. *J. Phys. Chem. C* **2008**, *112* (4), 951−957.
(63) Zhang, W.; Chen, M.; Gong, X.; Diao, G. Universal Water-Soluble Cyclodextrin Polymer-Carbon Nanomaterials with Supramolecular Recognition. *Carbon* **2013**, *61*, 154−163.
(64) Davis, J. T.; Spada, G. P. Supramolecular Architectures Generated by Self-Assembly of Guanosine Derivatives. *Chem. Soc. Rev.* **2007**, *36* (2), 296−313.
(65) Rotaru, A.; Pricope, G.; Plank, T. N.; Clima, L.; Ursu, E. L.; Pinteala, M.; Davis, J. T.; Barboiu, M. G-Quartet Hydrogels for Effective Cell Growth Applications. *Chem. Commun.* **2017**, *53* (94), 12668−12671.
(66) Shang, H.; Wu, J.; Liu, X.; Tong, Y.; He, Y.; Huang, Q.; Xia, D.; Peng, E.; Chen, Z.; Tang, K. Second Near-Infrared Nanomaterials for Cancer Photothermal Immunotherapy. *Mater. Today Adv.* **2023**, *17*, 100339.
(67) Li, Y.; Li, X.; Doughty, A.; West, C.; Wang, L.; Zhou, F.; Nordquist, R. E.; Chen, W. R. Phototherapy Using Immunologically Modified Carbon Nanotubes to Potentiate Checkpoint Blockade for Metastatic Breast Cancer. *Nanomed. Nanotechnol.* **2019**, *18*, 44−53.
(68) González-Rodríguez, L.; Pérez-Davila, S.; López-Álvarez, M.; Chiussi, S.; Serra, J.; González, P. Review Article Laser-Induced Hyperthermia on Graphene Oxide Composites. *J. Nanobiotechnol.* **2023**, *21* (1), 196.
(69) Shahnawaz Khan, M.; Abdelhamid, H. N.; Wu, H. F. Near Infrared (NIR) Laser Mediated Surface Activation of Graphene Oxide Nanoflakes for Efficient Antibacterial, Antifungal and Wound Healing Treatment. *Colloids Surf.* **2015**, *127*, 281−291.
(70) Robinson, J. T.; Tabakman, S. M.; Liang, Y.; Wang, H.; Sanchez Casalongue, H.; Vinh, D.; Dai, H. Ultrasmall Reduced Graphene Oxide with High Near-Infrared Absorbance for Photothermal Therapy. *J. Am. Chem. Soc.* **2011**, *133* (17), 6825−6831.
(71) Shanmugam, V.; Selvakumar, S.; Yeh, C.-S. Near-Infrared Light-Responsive Nanomaterials in Cancer Therapeutics. *Chem. Soc. Rev.* **2014**, *43* (17), 6254−6287.
(72) Markovic, Z. M.; Harhaji-Trajkovic, L. M.; Todorovic-Markovic, B. M.; Kepić, D. P.; Arsikin, K. M.; Jovanović, S. P.; Pantovic, A. C.; Dramićanin, M. D.; Trajkovic, V. S. In Vitro Comparison of the Photothermal Anticancer Activity of Graphene Nanoparticles and Carbon Nanotubes. *Biomaterials* **2011**, *32* (4), 1121−1129.
(73) Vaishampayan, A.; Grohmann, E. Antimicrobials Functioning through ROS-Mediated Mechanisms: Current Insights. *Microorganisms* **2021**, *10* (1), 61.
(74) Mohammed, H.; Kumar, A.; Bekyarova, E.; Al-Hadeethi, Y.; Zhang, X.; Chen, M.; Ansari, M. S.; Cochis, A.; Rimondini, L. Antimicrobial Mechanisms and Effectiveness of Graphene and Graphene-Functionalized Biomaterials. A Scope Review. *Front. Bioeng. Biotechnol.* **2020**, *8*, 465.
(75) Akhavan, O.; Ghaderi, E.; Esfandiar, A. Wrapping Bacteria by Graphene Nanosheets for Isolation from Environment, Reactivation by Sonication, and Inactivation by Near-Infrared Irradiation. *J. Phys. Chem. B* **2011**, *115* (19), 6279−6288.

https://doi.org/10.1021/acsomega.3c07724
ACS Omega 2024, 9, 15833−15844

(76) Liu, X.; Sen, S.; Liu, J.; Kulaots, I.; Geohegan, D.; Kane, A.; Puretzky, A. A.; Rouleau, C. M.; More, K. L.; Palmore, G. T. R.; Hurt, R. H. Antioxidant Deactivation on Graphenic Nanocarbon Surfaces. *Small* **2011**, *7* (19), 2775−2785.
(77) Carpio, I. E. M.; Santos, C. M.; Wei, X.; Rodrigues, D. F. Toxicity of a Polymer-Graphene Oxide Composite against Bacterial Planktonic Cells, Biofilms, and Mammalian Cells. *Nanoscale* **2012**, *4* (15), 4746−4756.
(78) Radhi, A.; Mohamad, D.; Rahman, F. S. A.; Abdullah, A. M.; Hasan, H. Mechanism and Factors Influence of Graphene-Based Nanomaterials Antimicrobial Activities and Application in Dentistry. *J. Mater. Res. Technol.* **2021**, *11*, 1290−1307.
(79) Kumar, P.; Huo, P.; Zhang, R.; Liu, B. Antibacterial Properties of Graphene-Based Nanomaterials. *Nanomaterials* **2019**, *9* (5), 737.
(80) Hu, W.; Peng, C.; Luo, W.; Lv, M.; Li, X.; Li, D.; Huang, Q.; Fan, C. Graphene-Based Antibacterial Paper. *ACS Nano* **2010**, *4* (7), 4317−4323.
(81) Ding, L.; Wang, H.; Liu, D.; Zeng, X.-A.; Mao, Y. Bacteria Capture and Inactivation with Functionalized Multi-Walled Carbon Nanotubes (MWCNTs). *J. Nanosci. Nanotechnol.* **2020**, *20* (4), 2055−2062.
(82) Azizi-Lalabadi, M.; Hashemi, H.; Feng, J.; Jafari, S. M. Carbon Nanomaterials against Pathogens; the Antimicrobial Activity of Carbon Nanotubes, Graphene/Graphene Oxide, Fullerenes, and Their Nanocomposites. *Adv. Colloid Interface Sci.* **2020**, *284*, 102250.
(83) Li, P.; Poon, Y. F.; Li, W.; Zhu, H.-Y.; Yeap, S. H.; Cao, Y.; Qi, X.; Zhou, C.; Lamrani, M.; Beuerman, R. W.; Kang, E.-T.; Mu, Y.; Li, C. M.; Chang, M. W.; Jan Leong, S. S.; Chan-Park, M. B. A Polycationic Antimicrobial and Biocompatible Hydrogel with Microbe Membrane Suctioning Ability. *Nat. Mater.* **2011**, *10* (2), 149−156.
(84) Saleemi, M. A.; Kong, Y. L.; Yong, P. V. C.; Wong, E. H. An Overview of Antimicrobial Properties of Carbon Nanotubes-Based Nanocomposites. *Adv. Pharm. Bull.* **2022**, *12* (3), 449−465.
(85) Liang, Y.; Zhao, X.; Hu, T.; Chen, B.; Yin, Z.; Ma, P. X.; Guo, B. Adhesive Hemostatic Conducting Injectable Composite Hydrogels with Sustained Drug Release and Photothermal Antibacterial Activity to Promote Full-Thickness Skin Regeneration During Wound Healing. *Small* **2019**, *15* (12), 1900046.
(86) Huang, S.; Liu, H.; Liao, K.; Hu, Q.; Guo, R.; Deng, K. Functionalized GO Nanovehicles with Nitric Oxide Release and Photothermal Activity-Based Hydrogels for Bacteria-Infected Wound Healing. *ACS Appl. Mater. Interfaces* **2020**, *12* (26), 28952−28964.
(87) Zhang, B.; He, J.; Shi, M.; Liang, Y.; Guo, B. Injectable Self-Healing Supramolecular Hydrogels with Conductivity and Photo-Thermal Antibacterial Activity to Enhance Complete Skin Regeneration. *Chem. Eng. J.* **2020**, *400*, 125994.
(88) Das, P. N.; Raj, K. G. Chitosan Coated Graphene Oxide Incorporated Sodium Alginate Hydrogel Beads for the Controlled Release of Amoxicillin. *Int. J. Biol. Macromol.* **2024**, *254*, 127837.
(89) Bellingeri, R.; Mulko, L.; Molina, M.; Picco, N.; Alustiza, F.; Grosso, C.; Vivas, A.; Acevedo, D. F.; Barbero, C. A. Nanocomposites Based on pH-Sensitive Hydrogels and Chitosan Decorated Carbon Nanotubes with Antibacterial Properties. *Mater. Sci. Eng. C* **2018**, *90*, 461−467.
(90) ISO 10993−5:2009 Biological Evaluation of Medical Devices. *Part 5: Tests for In Vitro Cytotoxicity*; International Organization for Standardization: Geneva, Switzerland, 2009.
(91) Zhou, Z.; Yan, D.; Cheng, X.; Kong, M.; Liu, Y.; Feng, C.; Chen, X. Biomaterials Based on N,N,N-Trimethyl Chitosan Fibers in Wound Dressing Applications. *Int. J. Biol. Macromol.* **2016**, *89*, 471−476.

https://doi.org/10.1021/acsomega.3c07724
ACS Omega 2024, 9, 15833−15844